Research Square

Preprints are preliminary reports that have not undergone peer review.
They should not be considered conclusive, used to inform clinical practice,
or referenced by the media as validated information.

Room-temperature printing of 2D GaN semiconductor via liquid metal gallium surface confined nitridation reaction

Jing Liu (jliu@mail.ipc.ac.cn)
Technical Institute of Physics and Chemistry, Chinese Academy of Sciences
Qian Li
Technical Institute of Physics and Chemistry Chinese Academy of Sciences
Bang-Deng Du
Technical Institute of Physics and Chemistry, Chinese Academy of Sciences
Jian-Ye Gao
Technical Institute of Physics and Chemistry, Chinese Academy of Sciences
Bao-Yu Xing
State Key Laboratory of Laser Propulsion and Application, Space Engineering University
Dian-Kai Wang
State Key Laboratory of Laser Propulsion and Application, Space Engineering University
Ji-Fei Ye
State Key Laboratory of Laser Propulsion and Application, Space Engineering University

Article

Keywords: 2D GaN semiconductor, liquid metal gallium surface-confined nitridation reaction, microelectronic devices

Posted Date: November 18th, 2021

DOI: https://doi.org/10.21203/rs.3.rs-1007329/v1

License: This work is licensed under a Creative Commons Attribution 4.0 International License.
Read Full License

Abstract

Outstanding wide-bandgap semiconductor materials like gallium nitride (GaN) have been extensively utilized in power electronics, radiofrequency power amplifiers, and harsh environment adaptability. Due to its quantum confinement impact in enabling desired deep-ultraviolet emission, excitonic impact, and electronic transport features, two-dimensional (2D) GaN has been one of the most remarkable areas for the future growth of microelectronic devices. Here, for the first time, we report a large area, wide bandgap, and room-temperature 2D GaN synthesis and printing strategy via liquid metal gallium surface-confined nitridation reaction. The developed low-temperature synthesis and printing process is consistent with various electronic device manufacturing methods and thus opens a way for the cost-effective growth of the third-generation semiconductor. In particular, the fully printed field-effect transistors relying on the GaN show p-type switching with an on/off ratio greater than 105, maximum field-effect hole mobility of 53 cm2 V−1 s−1, and a small sub-threshold swing at room temperature. The current study establishes a room temperature way to produce the GaN, which can be further verified, generalized, and realized for various upcoming electronic and photoelectronic applications.

1. Introduction

Semiconductor technology is the fundamental core of the integrated circuit industry. Since the bottleneck of the first two generations of semiconductors, the third-generation high-temperature wide-band-gap semiconductor nanomaterials like gallium nitride (GaN)[1], zinc oxide (ZnO), aluminum nitride (AlN)[2], silicon carbide (SiC)[3,4], and diamond, have been developed recently. GaN nanomaterials are novel semiconductor materials owning some benefits like high saturated electron mobility, radiation resistance, acid and alkali corrosion resistance, high thermal conductivity, and high breakdown field. In GaN electronic devices, the inevitable electron transfer from the valence band to the conduction band can be suppressed through the wide energy bandgap. The ambient energy from high electric fields, high temperature, and high-energy particles can activate the mentioned electron transfer[5]. Accordingly, the devices can retain their electrical features in various scenarios. The GaN is one of the most attractive semiconductor materials due to its outstanding efficiency and stability[6,7]. Various studies have been devoted to developing and analyzing the GAN materials in the literature[8–10].

Compared with the corresponding bulk GaN materials, various nanoscale effects of low dimensional GaN materials can show better photoelectric, mechanical, thermal stability, electrical[11,12], and chemical features[13]. Apart from the fundamental physicochemical features of GaN, they also have the surface, small-size, and quantum-confinement impacts as one of the exciting areas for future growth of microelectronic devices. However, it is not easy to construct a low-dimensional GaN. Syed et al. reported a two-step process to synthesis two-dimensional (2D) GaN nanosheets, the process includes obtaining 2D Ga_2O_3 by extrusion printing, and then converting Ga_2O_3 to GaN by ammonolysis in a tubular furnace[14]. Chen et al. reported the development of 2D GaN single crystals attained using a surface-confined nitridation reaction (SCNR) through the chemical vapor deposition (CVD)[15]. In 2016, Al Balushi et al.

employed the migration-enhanced encapsulated growth method to construct 2D GaN monolayer nanosheets[16]. However, the temperatures used in the most of process are above 500 °C that is inconsistent with various electronic industry operations. The long run time of the deposition process can increase the cost and feasibility. The construction and research technology of low-dimensional GaN materials and devices should be developed and enhanced to satisfy the appeals of practical applications. The low temperature preparation of large-area, high-quality and uniform GaN films will have a significant impact on high thermal stability 2D integrated circuit industry designed for power electronics applications. However, so far, there is still no report on the room temperature preparation of 2D GaN films.

Herein, we proposed and demonstrated for the first time to print the 2D GaN films on SiO_2/Si substrates through introducing a liquid metal-based synthesis and printing processes at room temperature. The process relies on using nitrogen plasma to trigger nitriding of gallium droplets at room temperature, and then transferring them to the substrate through the proposed van der Waals (vdW) printing technology. The whole preparation process is performed at room temperature that is consistent with the current manufacturing processes. The proposed method can produce monolayer, and multilayer GaN attained via individual or multiple prints, respectively. Morever, we report excellent electronic performance of the printed 2D GaN. Fully printed side-gated field-effect transistors (FETs) are fabricated, from which the 2D GaN-FETs exhibit outstanding performance with a large current on/off ratio (> 10^5), high field-effect mobility (~53 $cm^2 V^{-1} s^{-1}$), and tiny subthreshold slopes (~ 98 mV dec^{-1}) with a high degree of reproducibility. This study introduces a reliable and straightforward large-scale manufacturing technique for 2D GaN and its features, which opens great practical potential for wafer-scale processes. It also paves the way for the application of GaN semiconductor in a new generation of all printed electronic devices, integrated circuits and more functional devices.

2. Results And Discussion

Liquid metal-based 2D GaN printing technology. The schematic in Fig. 1a illustrates the preparation of ultrathin 2D GaN layer using N_2-plasma treatment technology at room temperature. The plasma nitriding process employs an unusual glow discharge involving high current and charge densities. A potential difference is generated by applying a DC voltage between the components (cathode) and the furnace walls (anode), which ionizes the treatment gas to produce the glow discharge. The treatment gas's positive ions speed up to the negatively connected parts and hit the surface with high kinetic energy, sputtering the surface and heating the whole parts. Nitrogen plasma is an electrically neutral aggregate composed of N^+, N_2^+, e and N_2 formed after nitrogen is ionized. In the plasma nitriding of gallium, nitrogen ions and accelerated neutral nitrogen atoms lie on the surface to construct a nitrogen-rich film that forms a nitride layer on the surface. Because the chemical reaction of nitrogen plasma is a thermodynamically stable excited state and ionic state, and the reaction activation energy is very low, it is much easier to generate GaN by the reaction of nitrogen plasma with liquid Ga than by the traditional nitriding reaction Ga $(CH_3)_3$ + NH_3 → GaN + $3CH_4$.

The schematic setup of the system to transform the liquid Ga to 2D GaN is elucidated in Fig. 1b. The formation of 2D GaN thin films was realized by nitrogen plasma triggering surface limited nitriding reaction. Gallium droplets with plasma treated surface were placed on SiO_2/Si substrate and moved on the surface with the help of scraper, during the scraping process of liquid Ga, the surface nitride produced by plasma bombardment in nitrogen environment sticks to the substrate through van der Waals force (Fig. 1c) (Detailed description of the process parameters will be given in the Methods.). The nitridation reaction and printing of Ga both are conducted at room temperature that is consistent with the current electronic device production processes. The covered substrate area can be expanded by choosing a larger droplet diameter and a longer travel distance of the scraper. The thickness of the film can be increased via frequent printing (Methods and Supplementary Fig. 2). Figure 1d revealed a large and continuous ultrathin GaN film reaching lateral dimensions more than many centimeters. Based on atomic force microscopy (AFM), the thickness of the deposited GaN layer is ~4 nm that is moderately greater than a single GaN unit cell (Fig. 1e). AFM also indicates that the printed GaN film's surface roughness is analogous to that of the SiO_2 substrate, demonstrating that the 2D GaN film has minimum cracks, holes, folds, or bubbles, reflecting conformal and homogeneous attachment. The uniform thickness in broad regions and numerous samples supports the proposed Cabrera–Mott growth mechanism, where concurrent nitrides are formed among the whole metal interface, resulting in self-limiting growth to an accurate thickness. The mentioned approach is highly reproducible for growing large-area GaN sheets because the process was terminated more than 50 times and always yielded identical, continuous, laterally extensive atomically thin GaN films with reproducible features. The GaN film was initially printed on the SiO_2/Si substrate, but further tests demonstrated that the formation of uniform centimeter-scale semiconductor films on various substrates could be reproduced through the printing technology, indicating that the presented construction approach is suitable to deposit 2D GaN for several materials. Moreover, it should be pointed out that this method is also applicable to the fabrication of GaN heterostructures. In order to be compatible with silicon-based electronic technology, the 2D film printed on SiO_2/Si surface should be employed for further description and device construction.

Properties of the 2D GaN. Transmission electron microscopy (TEM) can be utilized to verify the crystallographic features of printed 2D GaN. The 2D GaN films were immediately moved to a TEM grid since it was printed. A high-resolution TEM micrograph (HRTEM) and selective area electron diffraction (SAED) pattern of the GaN are presented in Fig. 2a and 2b, respectively, which confirms the crystallization of the printed GaN in the polymorph. The atomic spacing of 0.285 nm in the HRTEM image and the distance of the fringes at 0.266 nm correspond to the (100) and (002) planes of GaN, respectively, and that at 0.248 nm corresponds to the (101) plane.

The 2D GaN film's phonon modes also change compared to those for the bulk[17]. Based on the Raman spectra presented in Fig. 2c, two peaks at 561 and 735 cm^{-1} appear in 2D printed GaN, respectively, corresponding to E_1 (TO) and A_1 (LO) modes in the bulk phase. Moreover, the above distinction reflects the change in GaN's phonons modes in 2D limit, while its location at 566.2 cm^{-1} is blue-shifted comparing to that of the bulk, reflecting a tensile-strain state in the 2D limit[18]. The peak position of A_1

(LO) mode corresponds to 731 cm^{-1}, and there is a blue shift relative to the peak position of 736 cm^{-1} in the bulk phase. Generally speaking, the parameters influencing Raman scattering involve material size, order, internal stress and structural defects. Copwell et al.[19] believe that the reduction of nano material size will lead to the movement, broadening and asymmetric peak shape. In addition, the proposed spectrum lacks various Raman properties of Ga_2O_3 (i.e., peaks at ~167, ~320, ~344, and ~475 cm^{-1}), indicating that GaN is successfully constructed and Ga is quantitatively changed within plasma discharge nitriding reaction. It was observed that the Raman peak intensity for 456.6 cm^{-1} modes was notably decreased than that of the bulk counterpart, while the A_1 Raman mode is susceptible to the free charge carrier density in graphene and 2D metal chalcogenides[20–23]. Due to its broader bandgap, 2D GaN can involve further trap states. The appearance of more polar 2D GaN changes the interaction between phonon and free charge carriers, obtained by the trap states, inside the 2D material, resulting in phonon self-energy renormalization. Thus, phonons are attenuated, decreasing the charge-sensitive A_1 Raman mode's intensity[20–23].

X-ray photoelectron spectroscopy (XPS) is utilized to attain the printed 2D GaN's chemical bonding states. Figures 2d and e present the spectra of Ga 2p and N 1s areas for the GaN, respectively. The doublet in the Ga 2p region corresponds to the $2p_{3/2}$ and $2p_{1/2}$ orbital of Ga, the characteristic gallium peak for Ga_2O_3 placed at ~20.4 eV was not seen, indicating Ga's quantitative transformation. The principal broad N 1s peak centered at ~397.6 eV corresponds to the N 1s region compatible with the desired N 1s area presented in GaN. Energy-dispersive X-ray spectroscopy (EDS) mapping study of the resulting film composition (Supplementary Fig. 3) indicated that the deposited layer is mainly GaN with nitrogen to gallium ratio around 1, confirming the stoichiometric GaN. High-performance 2D semiconductors with a large area and good uniformity is necessary for empirical electronic device applications.

Gallium Nitride has a predicted bandgap in the range of 3.32 eV to 3.52 eV for the bulk and ultra-thin GaN, respectively. The obtained electronic band structure and density of states (DOS) of an individual unit cell of printed 2D GaN are shown in Fig. 3a. Vienna Ab initio Simulation Package (VASP, version: 5.4.4) combined with the projector augmented wave (PAW) approach were utilized to accomplish the first-principles computations[24–26]. The Perdew-Burke-Ernzerhof (PBE) functional integrated with the DFT-D3 correction was employed to treat the exchange-functional. The plane wave's cut-off energy was adjusted at 520 eV[27]. The Brillouin zone integration was accomplished with 15*15*6 Monkhorts-Pack point sampling to optimize the bulk GaN. The self-consistent computations can give a 10-4 eV convergence energy threshold. The optimal values of the equilibrium geometries and lattice constancies were obtained with maximum stress on all atoms in 0.01 eV/Å. For the GaN (110) surface structure, we use the 7*7*1 K-points for structural optimization and self-consistent calculations. Because the PBE functional will underestimate the band gap of the semiconductor, we also use the hybrid functional method (HSE06)[28] to calculate the band gap and DOS. Our density PBE functional analysis indicates that the GaN has a 1.51 eV direct bandgap. According to the HSE06 calculation, the printed 2D GaN has a 3.32 eV direct

bandgap. From Fig. 3b, the measured band gap derived from the UV-Vis absorption is 3.3 eV, which agrees well with the value derived from HSE06 calculation. By comparison, the calculated bandgap using energy density PBE functional analysis is smaller than the measurement result. Figure 3c shows a periodic slab of GaN with a non-polar (110) surface sliced from the wurtzite bulk phase.

Application of 2D GaN in electronic devices. For experimental assessment of the electron transport features of printed 2D GaN and to investigate the potential for electronic devices, field-effect transistors (FETs) were constructed to assess the 2D GaN for electronic device applications. Figure 4a shows the structure diagram of the transistor based on printed 2D GaN. We have adopted an individual side-gate design for all of the devices fabricated in this study, and detailed description of the fabrication process will be presented in the Methods section. Figure 4b presents a scanning electron microscopy (SEM) image of the device. Ag was used as gate electrodes and source–drain metal contacts, and FET channels were patterned with a width of W_{ch} = 1000 μm and the length of L_{ch} = 50 μm. Electrical measurements were carried out for the printed side-gated 2D GaN FET. Figure 4c presents the transfer (drain current, I_{ds}, with respect to the gate voltage, V_{gs}) features of a representative 2D GaN FET. Figure 4d presents the I_{ds} with respect to the drain–source voltage (V_{ds}) at various values of V_{gs} applied to the device. As presented in Fig. 4c and d, the printed 2D GaN FET devices' p-type switching feature with an on/off ratio is more than 10^5. The sub-threshold swing (SS) for the FET was 98 mV per decade, near the desired action. The average value of the room-temperature field-effect mobility (μ) was obtained as 53.1 $cm^2 V^{-1} s^{-1}$, with a mobility of 57 $cm^2 V^{-1} s^{-1}$ for the device with the best performance (The FET mobility computations are presented in the Supplementary Note 3). A statistical analysis of the performance of many FET devices on fabricated using the here reported wafer-scale printing process was conducted. Electrical features of thirty printed GaN FETs were evaluated. The mean log ON/OFF current ratio, mobility, and SS were 5.31 ± 0.52, 53.1 ± 4.5 $cm^2 V^{-1} s^{-1}$, and 97.6 ± 2.42 mV dec^{-1} (Fig. 4e-g), respectively. A desired was seen between various devices, considering that the mentioned devices were constructed in an academic laboratory. This uniformity yields confidence in employing the mentioned devices and methods in numerous applications like integrated circuits and active-matrix back-planes for displays. Moreover, the 2D GaN-based FETs were significantly stable, having a high cyclability with a stable on/off ratio and stable on currents for more than 100 switching cycles under ambient conditions (Supplementary Fig. 4).

Notably, the observed field-effect mobility is greater compared to that of traditional high-efficiency broad-bandgap GaN-based devices[14, 29]. For further broader comparison, Fig. 5 plots SS versus mobility for p-type and n-type FETs reported in the literature as well as the device from this study, the value of SS is comparable to that appeared in some of the best p-type and n-type oxide semiconductors like indium oxide, this highlights the fact that our approach offers a high current mobility while maintaining a small SS, which is mainly attributed to the high-quality electron-level GaN semiconductor. Besides, no detectable performance degradation was observed in the devices while working under ambient situations without encapsulation. This highlights that the printed GaN is of exceptional quality while indicating that additional enhancements can be achieved via the enhanced device construction. Future studies should concentrate on constructing devices that can integrate separately addressable transistors into more

complicated circuits. Potential approaches can involve using vdW heterostructures with dielectrics like hexagonal boron nitride or Ga_2O_3 combined with top gates[30, 31]. The mentioned device configurations can be employed to determine essential parameters like the pinch-off voltage that can be informative for incorporating future devices into functional circuits.

3. Conclusions

Liquid metals have various possible functionalities. The essential value of the mentioned materials is that they can serve as a reactive and templating media simultaneously and thus to synthesis and print a wide range of 2D semiconductor materials with extensive applications. In the current work, we presented the successful printing of the high-quality 2D GaN films with a large scale via a plasma nitridation reaction and through transferring occurring in the liquid metal's nitride skin constructed under this specific condition. Moreover, complete explanation and analysis have been performed on the electrical features of printed 2D GaN films, giving essential advice for further evolution of liquid metal printed high-performance semiconductors and indicating their considerable potential for future nanoelectronics.

Notably, we effectively presented the printed FET devices using 2D GaN for the first time, indicating significant field-effect mobility and relatively small values of SS, demonstrating an extremely steep subthreshold voltage switching behavior. This high-efficiency, simple, large-size, and cheap production process provides a new way for advancing GaN transistors for power electronics applications. Moreover, the 2D semiconductor can be produced as the favored material in printing different electronic devices due to the mentioned advantages. This sets up a new standard for subsequent electronics, sensors, and more practical devices. It also presents a pathway toward employing printed 2D high-efficiency semiconductors to construct novel electronic devices using liquid metal-enabled techniques.

4. Methods

Materials. Gallium with a purity of >99.99% was bought from Sigma Aldrich and utilized without additional refinement. The remaining materials were bought from usual suppliers and employed without refinement.

Formation of GaN on liquid gallium by nitridation reaction. In order to obtain 2D GaN films with high purity and low defects, the whole preparation and printing process were carried out in a glovebox in a pure N_2 environment at a pressure of 1 atm ~ 3 atm. The O_2 content in the glove box atmosphere is controlled below 3 ppm and the H_2O content is controlled below 0.5 ppm. High purity Ga was melted and then placed in NaOH solution to remove the oxide scale on the surface. The clean liquid Ga was extracted to 10 ml by a syringe and place it on the surface of the low-voltage electrode stainless steel plate of the plasma trigger device, and the stainless steel plate is grounded. In the environment of high purity N_2, it can be seen that the surface of liquid Ga is bright without any oxide film. The stainless steel disk wrapped in transparent quartz of plasma high-voltage electrode is suspended vertically above liquid Ga, and the distance between the disk and the surface of liquid Ga is about 1mm. A voltage of 50 kV is

applied between the two electrodes of the plasma trigger device through the voltage regulating device. At this time, the electric field strength of N_2 breakdown is 5×10^7 V m^{-1}, the output current is 16 A, and the uniform and dense GaN skin can be obtained on the liquid Ga surface after glow discharge treatment for a certain time.

Printing process of 2D GaN films. Wafers of 500 nm SiO_2 on Si (SiO_2/Si) were washed by the deionized (DI) water for 1 min, and then sonicated in acetone and isopropyl alcohol (IPA) for 10 min (25°C) and blown dry with N_2 gas. The 3 min of oxygen (O_2) plasma (Emitech K-1050X) at 100 W was then applied to wafers under the low vacuum (0.6 Torr). The nitrided Ga droplets was placed on the SiO_2/Si substrate and execute the complete printing program. The size of 2D nitride film changes with the droplet diameter and the travel distance of the scraper. The nitride layer formed on the liquid Ga's surface can be transformed and printed on the substrate by gently scraping the droplets from one end of the substrate to the other end with a scraper. An extra force within the extrusion phase can damage the nitride layer. By this extrusion printing method, high-quality GaN films with a transverse size greater than a few centimeters can be effectively printed on the substrate.

Mechanical and chemical cleaning process. In order to remove all liquid metal parts that remained on the sample, a facile mechanical ethanol cleaning method was employed. At first, around 100 ml of ethanol were taken in a beaker, and the beaker was heated on a heating plate to 100°C. Then, the substrate with printed 2D nitride film was immersed in hot ethanol with tweezers. In order to eliminate the metal residues, a wiping tool (swab) was utilized for wiping the substrate immersed in ethanol. Due to a strong vdW adhesion between the nitride film and the bottom layer, the nitride film still sticks to the silicon oxide surface within the wiping proceeding. Besides, the weak adherence between the deposited nitride layer, the liquid metal, and the film could be quickly removed to maintain the 2D film clean and intact. Moreover, a chemical process was employed to clean the samples for a complete elimination of the metal residue on the substrate. An Iodine/triiodide (I^-/I^{3-}) solution (100 mmol L^{-1} LiI and 5 mmol L^{-1} I_2) was constructed in ethanol and then located on a hot plate to heat up to 50 ℃. In order to eliminate metallic inclusions, a substrate printed with the 2D-GaN film was immersed in a heated I^-/I^{3-} solution for a time interval. At last, the residual etchant was removed by cleaning the sample in deionized water. The liquid metal particles can be successfully eliminated using the mentioned two cleaning processes.

FET fabrication. In order to construct fully printed side-gated 2D GaN FETs, firstly, part of the 2D GaN/SiO_2 region is etched with HF solution with concentration of 1mol L^{-1} for about 10 s. Then, the etching area was cleaned with ethanol, the clean Si of a certain area was obtained on the substrate. The Ag ink (Ag40X, UT Dots, Inc.) involved 40 wt % Ag nanoparticles, with about 20 nm particle diameters, dispersed in a solvent mixture of xylene and terpineol (9:1 by volume). The constructed ink was printed on the 2D GaN films and SiO_2/Si substrates. A scientific 3B inkjet printer from Prtronic was adopted to verify the inkjet printing details. The obtained sample was located on the inkjet printer's panel at room temperature. A target image file was applied to the computer, which could be converted into a printable file through the software. Under computer control, source/drain electrodes and side-gate electrodes were

subsequently patterned by printing Ag on the substrate. Finally, the printed samples were then sedimented at 120°C in the air for 30 min in a furnace (MDL 281, Fisher Scientific Co.) to improve the conductivity.

Characterization.

The AFM images were employed by a Bruker Dimension Icon with “Scanasyst-air” AFM tips. A JEOL 2100F TEM/STEM (2011) system working at a 200 kV acceleration voltage involving a bright-field Gatan OneView 4k charge-coupled device (CCD) camera was utilized for both the low-resolution HRTEM imaging and SAED. A laser micro-Raman spectrometer (Renishaw in Via, 532 nm excitation wavelength) was adopted to accomplish the Raman spectroscopy. Moreover, the energy dispersive X-ray spectroscopic (EDS) measurements were used to collect the elemental mapping of the as-prepared samples. A thermo Scientific K-alpha XPS spectrometer associated with monochromatic X-rays from an Al anode (hv=~1486.6 eV) was adopted to perform the XPS analysis. A UV–visible (UV–vis) absorbance spectrometer (Hitachi U3900 UV–vis spectrophotometer) was utilized to evaluate the film’s optical bandgaps. A Cascade Microtech Summit 12000 semiautomated probe station linked to a Keithley 4200 Semiconductor Device Analyzer was adopted to measure 2D GaN FETs at room temperature.

Declarations

Acknowledgements

This work was partially supported by the National Natural Science Foundation of China under Grants No. 51890893 and 91748206.

Author contributions

The project was designed and directed by J. L. Q. L. and B. D. D. developed the synthesis and printing procedure for 2D GaN while also conducting the structure and properties measurements. B.D.D., B.Y.X., D.K.W. and J.F.Y. desinged nitrogen plasma and synthesised GaN on liquid metal Ga. Q. L. led the device fabrication with contributions from B. D. D. and J. Y. G., Q. L. and B. D. D. characterized the FET devices. Q. L analyzed the material and device characteristics and drafted the manuscript. All authors revised the manuscript.

Competing interests

The authors declare no competing interests.

References

1. Sanders, N., Bayerl, D., Shi, G., Mengle, K. A. & Kioupakis, E. Electronic and optical properties of two-dimensional GaN from first-principles. *Nano Lett.* **17**, 7345–7349 (2017).

2. Mansurov, V., Malina, T., Galitsyn, Yu. & Zhuravlev, K. Graphene-like AlN layer formation on (111) Si surface by ammonia molecular beam epitaxy. *J. Cryst. Growth.* **428**, 93–97 (2015).
3. Xu, L. et al. Rationally Designed 2D/2D SiC/g-C_3N_4 photocatalysts for hydrogen production. *Catal. Sci. Technol.* **9**, 3896–3906 (2019).
4. Li, Q., Xu, L., Luo, K. W., Wang, L. L. & Li, X. F. SiC/MoS_2 layered heterostructures: Promising photocatalysts revealed by a first-principles study. *Mat. Chem. Phys.* **216**, 64–71 (2018).
5. Khanna, S. M., Webb, J., Tang, H., Houdayer, A. J. & Carlone, C. 2 MeV proton radiation damage studies of gallium nitride films through low temperature photoluminescence spectroscopy measurements. *IEEE Trans. Nucl. Sci.* **47**, 2322–2328 (2000).
6. Luo, K. W., Xu, L., Wang, L. L. Li, Q. & Wang, Z. Ferromagnetism in zigzag GaN nanoribbons with tunable half-metallic gap. *Comput. Mater. Sci.* **117**, 300–305, (2016).
7. Zhu, Y., Li, H., Chen, T., Liu, D. & Zhou, Q. Investigation of the electronic and magnetic properties of low-dimensional $FeCl_2$ derivatives by first-principles calculations. *Vacuum* **182**, 109694 (2020).
8. Kolobov, A. V., Fons, P., Tominaga, J., Hyot, B. & André, B. Instability and spontaneous reconstruction of few-monolayer thick GaN graphitic structures. *Nano Lett.* **16**, 4849–4856 (2016).
9. Nakamura, S. Nobel Lecture: Background story of the invention of efficient blue InGaN light emitting diodes. *Rev. Mod. Phys.* **87**, 1139 (2015).
10. Xiao, W. -Z. et al. Ferromagnetic and metallic properties of the semihydrogenated GaN sheet. *Phys. Status Solidi B* **248**, 1442–1445 (2011).
11. Zhang, J., Sun, C. & Xu, K. Modulation of the electronic and magnetic properties of a GaN nanoribbon from dangling bonds. *Sci. China Phys. Mech. Astron.* **55**, 631–638 (2012).
12. Kandalam, A. K. et al. First principles study of polyatomic clusters of AlN, GaN, and InN. 1. Structure, stability, vibrations, and ionization. *J. Phys. Chem. B* **104**, 4361–4367 (2020).
13. Onen, A., Kecik, D., Durgun, E. & Ciraci, S. Onset of vertical bonds in new GaN multilayers: beyond van der Waals solids. *Nanoscale* **10**, 21842–21850 (2018).
14. Syed, N. et al. Wafer-sized ultrathin gallium and indium nitride nanosheets through the ammonolysis of liquid metal derived oxides. *J. Am. Chem. Soc.* **141**, 104–108 (2019).
15. Chen, Y. et al. Growth of 2D GaN single crystals on liquid metals. *J. Am. Chem. Soc.* **140**, 16392–16395 (2018).
16. Balushi, Z. Y. Al. et al. Two-dimensional gallium nitride realized via graphene encapsulation. *Nat Mater.* **15**, 1166–1171 (2016).
17. Caldwell, J. D. et al. Atomic-scale photonic hybrids for mid-infrared and terahertz nanophotonics. *Nat. Nanotechnol.* **11**, 9–15 (2016).
18. Glavin, N. R. et al. Flexible gallium nitride for high-performance, strainable radio-frequency devices. *Adv. Mater.* **29**, 1701838 (2017).
19. Campbell, I. H. & Fauchet, P. M. The effects of microcrystal size and shape on the one phonon Raman spectra of crystalline semiconductors. *Solid State Communications*, **58**, 739–741 (1986).

20. Liu, J. et al. The dependence of graphene Raman D-band on carrier density. *Nano Lett.* **13**, 6170–6175 (2013).
21. Voggu, R., Das, B., Rout, C. S. & Rao, C. N. R. Effects of charge transfer interaction of graphene with electron donor and acceptor molecules examined using Raman spectroscopy and cognate techniques. *J. Phys. Condens. Matter* **20**, 472204 (2008).
22. Shi, Y. et al. Selective decoration of Au nanoparticles on monolayer MoS_2 single crystals. *Sci. Rep.* **3**, 1839 (2013).
23. Ou, J. Z. et al. Physisorption-based charge transfer in two-dimensional SnS_2 for selective and reversible NO_2 gas sensing. *ACS Nano* **9**, 10313–10323 (2015).
24. Kresse, G. & Furthmüller, J. Efficient iterative schemes for ab initio total-energy calculations using a plane-wave basis set. *Phys. Rev. B* **54**, 11169 (1996).
25. Paier, J., Marsman, M., Hummer, K. & Kresse, G. Screened hybrid density functionals applied to solids. *J. Chem. Phys.* **124**, 154709 (2006).
26. Blöchl, P. E. Projector augmented-wave method. *Phys. Rev. B* **50**, 17953, (1994).
27. Jain, A. et al. Commentary: The materials project: A materials genome approach to accelerating materials innovation. *APL Materials* **1**, 011002 (2013).
28. Heyd, J. & Scuseria, G. E. Hybrid functionals based on a screened Coulomb potential. *J. Chem. Phys.* **118**, 8207 (2003).
29. Zheng, Z. et al. Gallium nitride-based complementary logic integrated circuits. *Nat Electron* **4**, 595–603 (2021).
30. Wurdack, M. et al. Ultrathin Ga_2O_3 glass: A large-scale passivation and protection material for monolayer WS_2. *Adv. Mater.* **33**, 2005732 (2020).
31. Lee, G.-H. et al. Highly stable, dual-gated MoS_2 transistors encapsulated by hexagonal boron nitride with gate-controllable contact, resistance and threshold voltage. *ACS Nano* **9**, 7019–7026 (2015).
32. Xu, W. et al. P-type transparent amorphous oxide thin-film transistors using low-temperature solution-processed nickel oxide. *J. Alloys Compd.* **806**, 40–51 (2019).
33. Shan, F. et al. High-mobility p-type NiOx thin-film transistors processed at low temperatures with Al_2O_3 high-k dielectric. *J. Mater. Chem. C.* **4**, 9438–9444 (2016).
34. Hu, H., Zhu, J., Chen, M., Guo, T. & Li, F. Inkjet-printed p-type nickel oxide thin-film transistor. *Appl. Surf. Sci.* **441**, 295–302 (2018).
35. Liu, A. et al. In situ one-step synthesis of p-type copper oxide for low-temperature, solution processed thin-film transistors. *J. Mater. Chem. C.* **5**, 2524–2530 (2017).
36. Yim, S. et al. Lanthanum doping enabling high drain current modulation in a p-type tin monoxide thin-film transistor. *ACS Appl. Mater. Interfaces* **11**, 47025–47036 (2019).
37. Li, S. et al. Preparation and characterization of solution-processed nanocrystalline p-type $CuAlO_2$ thin-film transistors. *Nanoscale Res. Lett.* **13**, 259 (2018).

38. Nie, S. et al. Solution-processed ternary p-type $CuCrO_2$ semiconductor thin films and their application in transistors. *J. Mater. Chem. C.* **6**, 1393–1398 (2018).
39. Ding, Y. et al. High-performance indium oxide thin-film transistors with aluminum oxide passivation. *IEEE Electron Device Lett.* **40**, 1949–1952 (2019).
40. Leppäniemi, J., Huttunen, O. -H., Majumdar, H. & Alastalo, A. Flexography-printed In_2O_3 semiconductor layers for high-mobility thin-film transistors on flexible plastic substrate. *Adv. Mater.* **27**, 7168–7175 (2015).
41. Lee, W. Y. et al. Densification control as a method of improving the ambient stability of solgel-processed SnO_2 thin-film transistors. *IEEE Electron Device Lett.* **40**, 905–908 (2019).
42. Zhang, L. et al. Structural, chemical, optical, and electrical evolution of solution-processed SnO_2 films and their applications in thin-film transistors. *J. Phys. D: Appl. Phys.* **53**, 175106 (2020).
43. Liang, D. -D., Zhang, Y. -Q., Cho, H. J. & Ohta, H. Electric field thermopower modulation analyses of the operation mechanism of transparent amorphous SnO_2 thin-film transistor. *Appl. Phys. Lett.* **116**, 143503 (2020).
44. Saha, J. K. et al. Highly stable, nanocrystalline, ZnO thin-film transistor by spray pyrolysis using high-k dielectric. *IEEE Trans. Electron Devices* **67**, 1021–1026 (2020).
45. Xu, W. et al. Low temperature solution-processed IGZO thin-film transistors. *Appl. Surf. Sci.* **455**, 554–560 (2018).
46. Messalea, K. A. et al. Two-step synthesis of large-area 2D Bi_2S_3 nanosheets featuring high in-plane anisotropy. *Adv. Mater. Interfaces* **7**, 2001131 (2020).

Figures

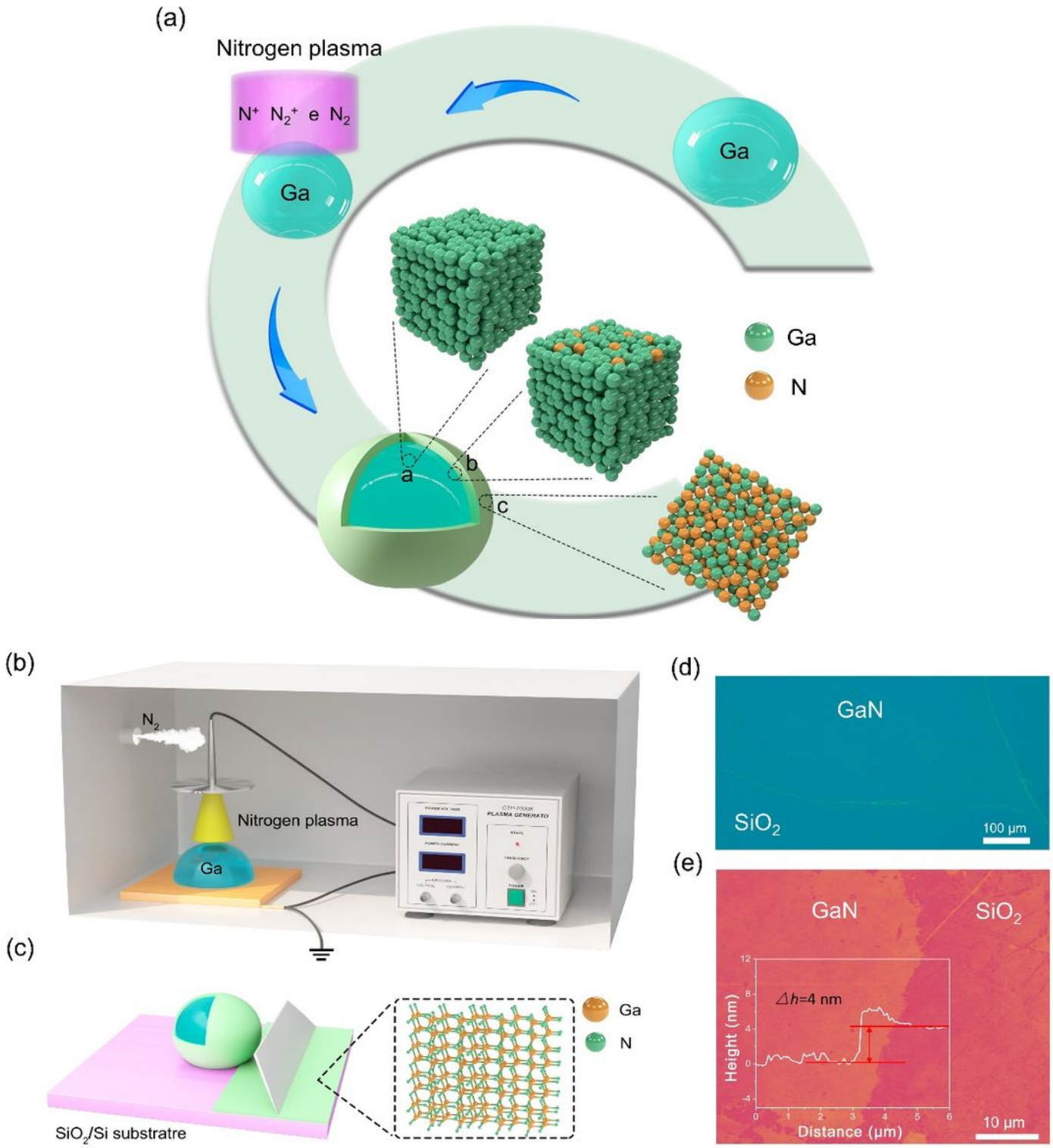

Figure 1

Schematic of the 2D GaN synthesis and printing process. (a) Schematic illustration of formation of surface nitride layer on liquid metals Ga via nitrogen-plasma reaction mechanism. a: Ga featuring disordered atoms, b: Ga-N bond formation at the liquid Ga surface, c: GaN layer. (b) Setup for the self-constructed plasma system used for producing GaN from liquid metal Ga. (c) Schematic description of the vdW 2D printing method of GaN film. The surface nitride of liquid Ga attaches to the substrate and

leaves 2D GaN on the surface. The figure on the right summarizes the crystal structure of 2D GaN film. (d) An optical image of the printed GaN layer with some square millimeters in lateral size. (e) AFM image of a printed GaN layer on a SiO2/Si wafer. The inset presents a step height profile with a 4 nm thickness.

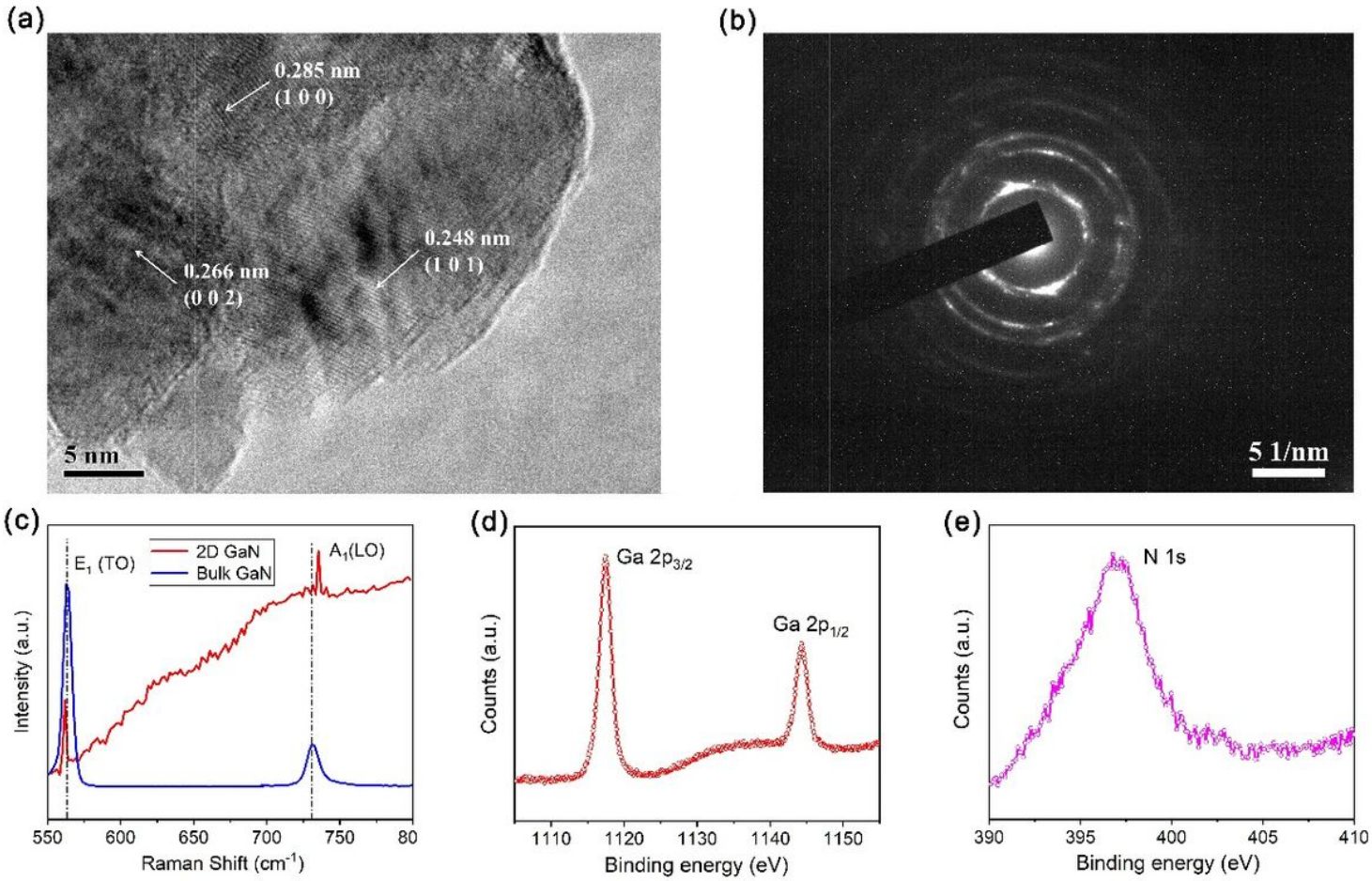

Figure 2

Description of the printed 2D GaN. (a) High-resolution TEM images of GaN directly laminated to a TEM grid. (b) Indexed chosen region's diffraction pattern for 2D GaN, demonstrating the polycrystalline structure of GaN. (c) Raman spectra for the bulk GaN and the 2D GaN with a 4.0 nm thickness, which present the areas of the E1 and A1 model peaks for the sample. (d, e) XPS results of the 2D GaN for the selected areas, (d) Ga 2p and (e) N 1s. The characteristic doublets for the Ga 2p area, 2p1/2, and 2p3/2, are located at ~1144.8 and ~1118.1 eV. The broad N 1s peak located at ~397.6 eV corresponds to the desired binding energy for nitrogen in GaN.

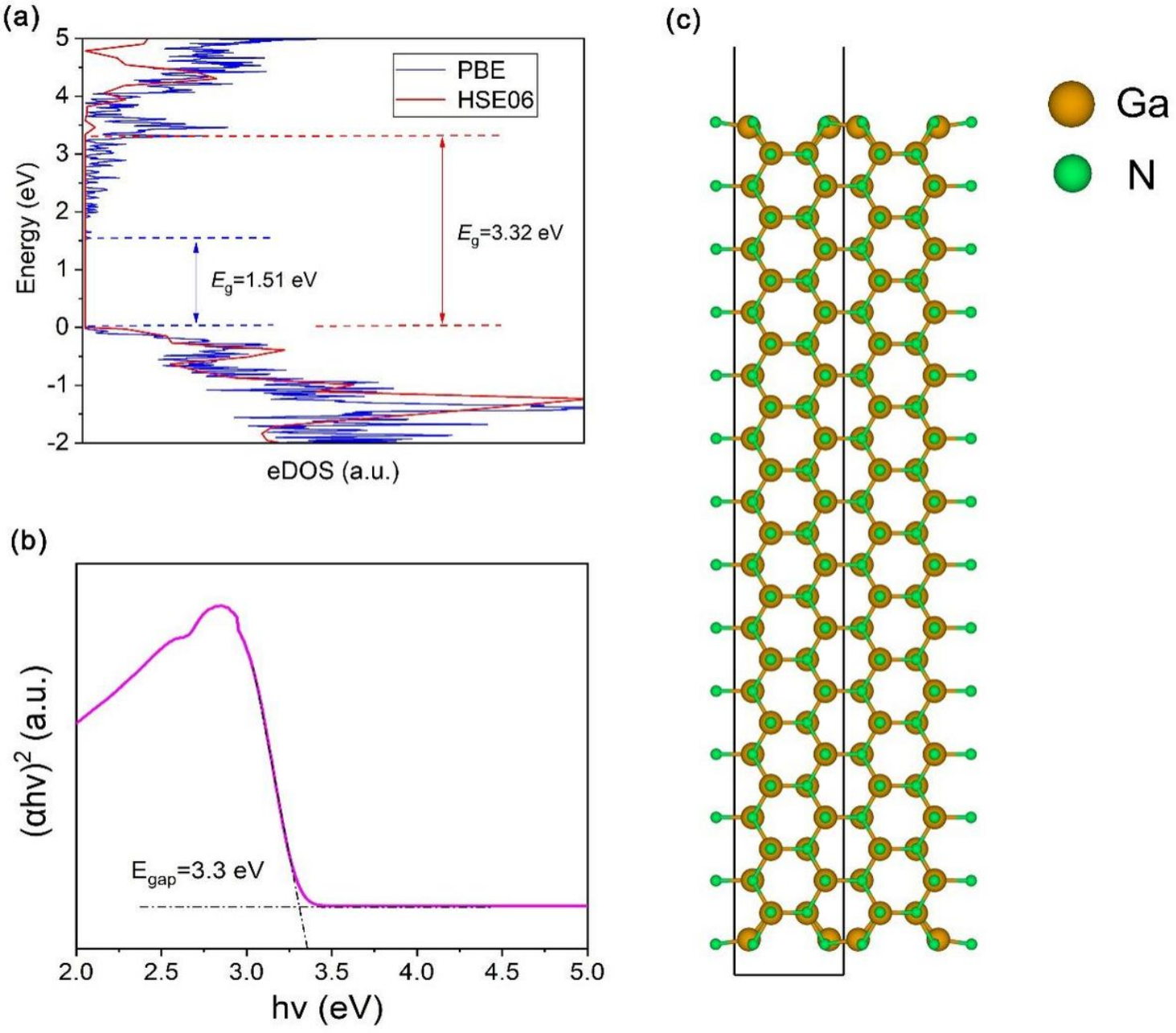

Figure 3

Electronic band descriptions of the printed 2D GaN. (a) Calculated electronic DOS of printed 2D GaN using PBE and HSE06 functional. (b) Tauc plot employed for ascertaining the electronic bandgap for GaN revealed a bandgap of 3.3 eV. (c) GaN (110) slab.

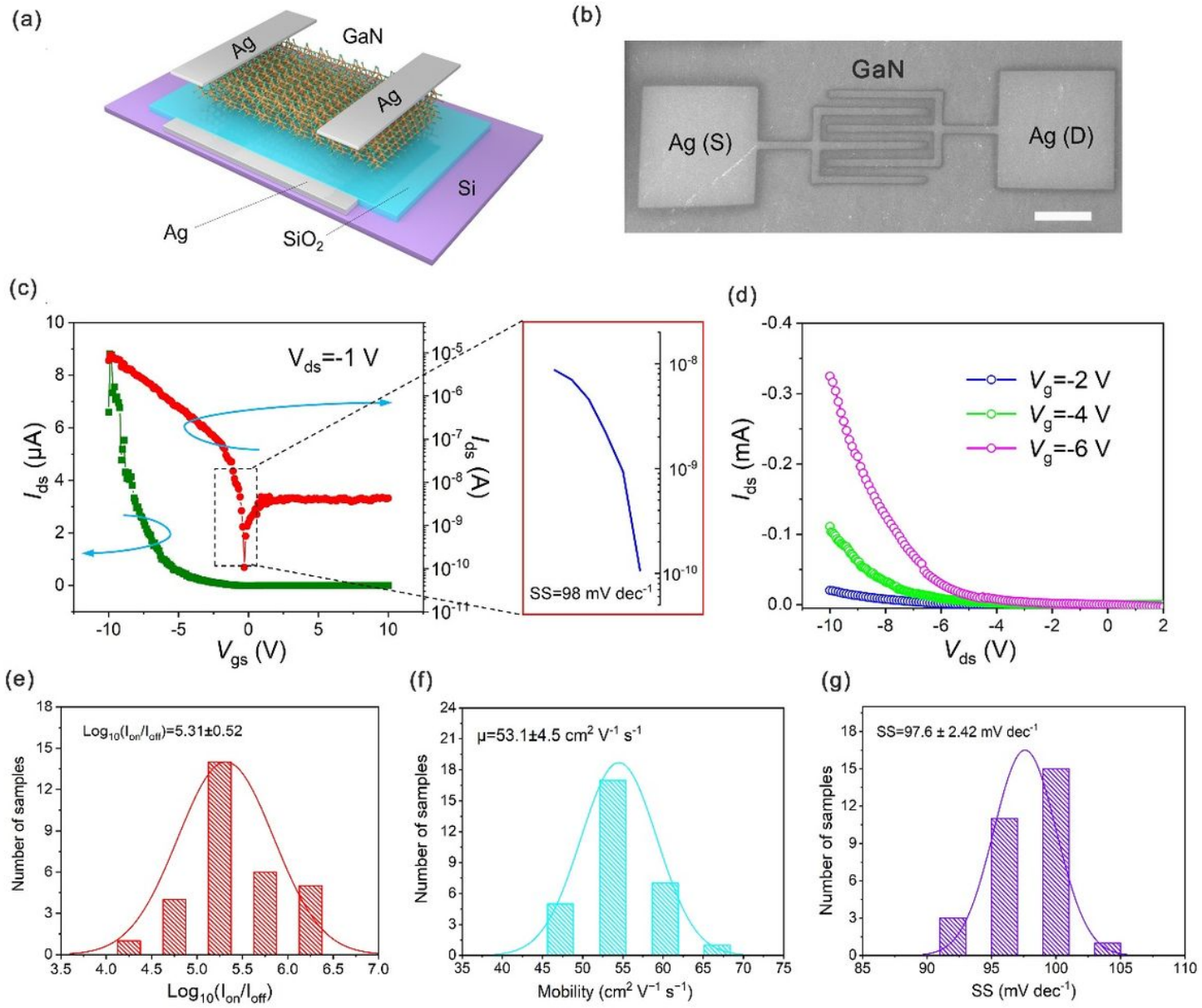

Figure 4

The printed GaN's field-effect transistor measurements. (a) Schematic of the device presenting a Si side-gated FET with silver source–drain electrodes. (b) The device's SEM image of the device. The scale bar corresponds to 500 μm. (c) Corresponding Ids–Vgs curve at Vds = − 1 V, showing a high Ion/Ioff ratio more than 105, small subthreshold slope of SS = 98 mV dec−1, yielding a field-effect mobility of μ = 53.1 cm2 V−1 s−1. (d) Set of Ids–Vds output curves from an individual FET, showing a large on current density of > 0.3 mA. Histograms of the (e) Log of the ON/OFF current ratio, (f) field-effect mobility and (g) subthreshold slope (SS) for 30 FETs.

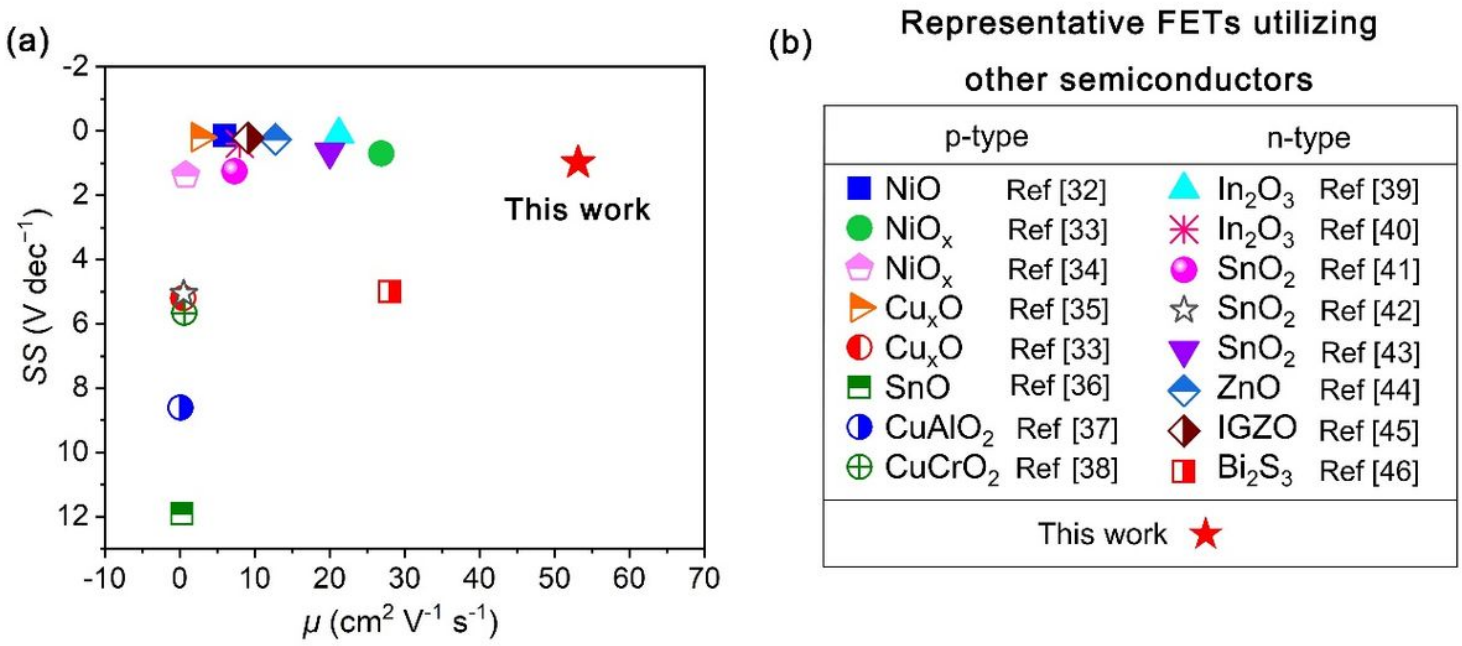

Figure 5

Field-effect transistor measurements of printed GaN. (a) Plot of subthreshold slope versus field-effect mobility to compare representative FETs reported in the literature. Our device shows the highest mobility while maintaining a small SS. (b) Legend for previously reported FETs utilizing p-type or n-type semiconductors for all plots.

Supplementary Files

This is a list of supplementary files associated with this preprint. Click to download.

- GaNSI.docx